PHYSICAL REVIEW D **94,** 086005 (2016)

Conductivities in an anisotropic medium

Sunly Khimphun,[1,*] Bum-Hoon Lee,[1,2,†] and Chanyong Park[2,3,‡]
[1]*Department of Physics, Sogang University, Seoul 121-742, Korea*
[2]*Asia Pacific Center for Theoretical Physics, Pohang 790-784, Korea*
[3]*Department of Physics, Postech, Pohang 790-784, Korea*
(Received 13 May 2016; published 14 October 2016)

In order to imitate the anisotropic medium of a condensed matter system, we take into account an Einstein-Maxwell-dilaton-axion model as a dual gravity theory where the anisotropy is caused by different momentum relaxations. This gravity model allows an anisotropic charged black hole solution. On this background, we investigate how the linear responses of vector modes like electric, thermoelectric, and thermal conductivities rely on the anisotropy. We find that the electric conductivity in the low frequency limit shows a Drude peak and that, in the intermediate frequency regime, it reveals the power law behavior. Specifically, when the anisotropy increases, the exponent of the power law becomes smaller. In addition, we find that a critical value for the anisotropy exists at which the dc conductivity reaches to its maximum value.

DOI: 10.1103/PhysRevD.94.086005

I. INTRODUCTION

Recently, considerable attention has been paid to the AdS/CFT correspondence (or holography) for understanding strongly interacting systems of nuclear and condensed matter physics. In the strong coupling regime, the traditional, well-established perturbation method does not work, so new physical concepts and/or mathematical techniques are required to figure out strongly interacting systems. In this situation, the AdS/CFT correspondence provides a new way to investigate it nonperturbatively. The AdS/CFT correspondence says that nonperturbative properties of a strongly interacting system can be described by a classical gravity theory defined on an asymptotic AdS geometry [1–4], which has already passed many nontrivial tests. In condensed matter physics describing a strongly interacting many-body system, there are many nontrivial, important properties, like a high T_c superconductivity and scaling behaviors of transport coefficients, depending on the phase of matter [5–8]. Understanding such properties theoretically, though it is not easy, is one of the long-standing problems in physics. After the AdS/CFT correspondence conjecture, there have been numerous attempts to resolve these issues via holographic techniques. In this work, we will study holographically various conductivities of a strongly interacting anisotropic medium and investigate how the anisotropy affects them.

When studying transport coefficients by using the holographic method, it is well known that if a translation symmetry exists, the electric conductivity shows a delta function behavior in the zero frequency limit. This fact means that the dc conductivity is not well defined in a system with a translational symmetry. To resolve this problem, many ideas for breaking the translational invariance of the dual gravity have been invented. The first is to encode the lattice structure to the anti–de Sitter (AdS) geometry, which is done by introducing a periodic potential along spatial directions [9–11]. Though this construction can describe the lattice structure of the dual theory, studying its transport coefficients is not easy because of the complexity of the model. Another way to consider the lattice structure is to impose the periodic boundary condition on the chemical potential, which is dual to a local gauge field of a dual gravity [12–15]. One can also take into account a massive gravity theory to break a diffeomorphism invariance [16–19]. Another way to break the translational symmetry is by introducing additional fields depending on spatial coordinates [20,21]. If we introduce scalar fields depending on spatial coordinates linearly, it can mimic the local point of the previous lattice structure. However, since the last method provides a relatively simple calculation, it would be a good toy model to understand the transport coefficients of the dual condensed matter system. From now on, we will focus on the last model.

In condensed matter and particle accelerator experiments, anisotropy is one of the important ingredients for understanding their physics. There were plenty of works related to the temporal and spatial anisotropies [20–31]. The spatial anisotropy naturally appears by breaking the rotational symmetry of the system. In the last model, this can be easily accomplished by taking different momentum relaxation parameters in the x and y directions. On the gravity side, this corresponds to introducing anisotropic axion fields. The gravity we will consider has a local gauge

*kpslourk@yahoo.com
†bhl@sogang.ac.kr
‡chanyong.park@apctp.org

field, a dilaton, and axions. In the AdS/CFT contexts, the local bulk gauge field can be identified with the matter with the corresponding global symmetry, while the dilaton field is mapped to the coupling constant of the dual field theory. From these facts, one can expect that the dual field theory of the above gravity describes a medium composed of strongly interacting matter. Adding anisotropic axions to this system, the dual system is modified to an anisotropic medium with different momentum relaxations. In order to clarify properties of the anisotropic medium, we study various conductivities by turning on vector fluctuations in this background geometry. We investigate how the anisotropy affects the transport coefficient, such as through various conductivities.

The rest of the paper is organized as follows. In Sec. II, we construct a dual charged black hole geometry of an anisotropic medium with different momentum relaxations. After turning on vector fluctuations in this background, we investigate the linear responses of the anisotropic medium in Sec. III. We finish this work with some concluding remarks in Sec. IV.

II. EINSTEIN-MAXWELL-DILATON-AXION MODEL

In order to study holographic linear response theory with an anisotropy, let us consider the following action:

$$S = \int d^4x\sqrt{-g}\Big(R + \frac{6}{L^2} - 2(\nabla\phi)^2 - \frac{1}{2}e^{4\phi}\sum_{i=1}^{2}(\nabla\tilde{a}_i)^2 - e^{-2\phi}F^2\Big), \tag{1}$$

where ϕ and $\tilde{a}_i$ represent a dynamical dilaton and two axion fields and L is the AdS radius. Following the AdS/CFT correspondence, the profile of the dilaton field can be reinterpreted as a nontrivial running scaling [32–37], while the bulk gauge field describes a certain fermionic matter, like a quark [38]. This means that the gravity theory we consider mimics a nonconformal medium composed of fermions and gauge bosons [39,40]. If we introduce the momentum relaxation with an anisotropy by turning on the axion fields, the dual field theory can further represent the anisotropic medium we are interested in. In order to describe a momentum relaxation, let us focus on the linear axion fields

$$\tilde{a}_1 = \alpha_1 x \qquad \tilde{a}_2 = \alpha_2 y, \tag{2}$$

where α_1 and α_2 are free parameters denoting the momentum relaxation. It is well known that, if there are no such axion fields, a dc conductivity generally diverges due to the translational symmetry. On the other hand, a momentum relaxation breaks the translational symmetry and leads to a finite dc conductivity. Thus, the existence of an axion field plays an important role in studying a transport coefficient like a dc conductivity. Above, we introduced two axion fields to break the translation symmetries in the x and y directions. For $\alpha_1 \neq \alpha_2$, the rotational symmetry is broken, while it is restored only when $\alpha_1 = \alpha_2$. For the isotropic case, various transport coefficients have been widely investigated (see [5–7,41–43] and the references therein). However, many samples in condensed matter experiments show an anisotropy. Therefore, it would be interesting to realize such an anisotropy ($\Delta\alpha \equiv |\alpha_1 - \alpha_2|$) in a holographic model and to investigate its properties.

Equations of motion governing the bulk fields are given by

$$R_{\mu\nu} = -\frac{3}{L^2}g_{\mu\nu} + 2\nabla_\mu\phi\nabla_\nu\phi + \frac{1}{2}e^{4\phi}\nabla_\mu\tilde{a}\nabla_\nu\tilde{a} + 2e^{-2\phi}F_{\mu\rho}F_\nu{}^\rho - \frac{1}{2}g_{\mu\nu}e^{-2\phi}F^2, \tag{3}$$

$$\Box\phi - \frac{1}{2}e^{4\phi}\sum_{i=1}^{2}(\nabla\tilde{a}_i)^2 + \frac{1}{2}e^{-2\phi}F^2 = 0, \tag{4}$$

$$\Box\tilde{a}_i + 4\nabla_\mu\phi\nabla^\mu\tilde{a}_i = 0, \tag{5}$$

$$\nabla_\mu(e^{-2\phi}F^{\mu\nu}) = 0. \tag{6}$$

When a rotational symmetry is broken, a general metric ansatz for a black hole has the following form [25,42]:

$$ds^2 = \frac{L^2}{z^2}(-g(z)dt^2 + g(z)^{-1}dz^2 + e^{A(z)+B(z)}dx^2 + e^{A(z)-B(z)}dy^2). \tag{7}$$

Assuming that the dilaton and the time component of the gauge field are functions of the radial coordinate only,

$$\phi = \phi(z), \quad \text{and} \quad A_\mu dx^\mu = A_t(z)dt, \tag{8}$$

Eq. (6) yields

$$F_{zt} = A_t' = \rho_z L e^{-A+2\phi}, \tag{9}$$

where ρ_z indicates a conserved charge density. Substituting this solution into the other equations, the remaining variables, $A(z)$, $B(z)$, and $\phi(z)$, are governed by

$$
\begin{aligned}
2A'' + (A')^2 + (B')^2 + 4(\phi')^2 &= 0, \\
gzB'' + (g(zA' - 2) + zg')B' + \frac{1}{2}ze^{-A-B+4\phi}(\alpha_1^2 - \alpha_2^2 e^{2B}) &= 0, \\
(4z - 2z^2A')g' + (-z^2(A')^2 + 8zA' + z^2(B')^2 + 4z^2(\phi')^2 - 12)g & \\
-\alpha_1^2 z^2 e^{-A-B+4\phi} - \alpha_2^2 z^2 e^{-A+B+4\phi} - 4\rho_z^2 z^4 e^{2\phi-2A} + 12 &= 0, \\
e^A g\phi'' + \left(e^A gA' + e^A g' - \frac{2e^A g}{z}\right)\phi' - \rho_z^2 z^2 e^{2\phi-A} - \frac{1}{2}\alpha_1^2 e^{4\phi-B} - \frac{1}{2}\alpha_2^2 e^{B+4\phi} &= 0.
\end{aligned} \tag{10}
$$

Note that the equation governing the dynamics of $g(z)$ is not independent.

Before solving these equations, it is worth noting that the action we considered is invariant under the following field redefinition:

$$
\begin{aligned}
&\phi \to \phi - \phi_0, \qquad \tilde{a}_1 \to e^{2\phi_0}\tilde{a}_1, \\
&\tilde{a}_2 \to e^{2\phi_0}\tilde{a}_2, \quad \text{and} \quad A_t \to e^{-\phi_0}A_t,
\end{aligned} \tag{11}
$$

where ϕ_0 implies a constant shift of the dilaton field. Additionally, the metric we have chosen is invariant under the following global scaling:

$$
\begin{aligned}
&A(z) \to A(z) + A(0), \quad B(z) \to B(z) + B(0), \\
&x \to e^{-(A(0)+B(0))/2}x, \quad \text{and} \quad y \to e^{-(A(0)-B(0))/2}y,
\end{aligned} \tag{12}
$$

where $A(0)$ and $B(0)$ indicate the boundary values of $A(z)$ and $B(z)$, respectively. These three constant shifts imply that one can take arbitrary values of A, B, and ϕ at a given z position, at either the horizon or the asymptotic boundary. In order to see that, let us first introduce a dimensionless coordinate scaled by the black hole horizon, $\tilde{z} = z/z_h$. Then the black hole horizon appears at $\tilde{z} = 1$. From now on, we will always use the $\tilde{z}$ coordinate, so we drop the tilde out for simplicity. Because of constant shifts of variables, we can set, without loss of generality,

$$
A(1) = B(1) = \phi(1) = 0. \tag{13}
$$

Note that the black hole factor should vanish at the horizon

$$
g(1) = 0. \tag{14}
$$

Substituting these values into equations of motion, the first derivatives of variables at the horizon must satisfy the following relations:

$$
\begin{aligned}
&A'(1) = -\frac{12 - 4\rho_z^2 - \alpha_1^2 - \alpha_2^2 - 4\kappa}{2\kappa}, \quad B'(1) = \frac{\alpha_1^2 - \alpha_2^2}{2\kappa}, \\
&\phi'(1) = \frac{-2\rho_z^2 - \alpha_1^2 - \alpha_2^2}{2\kappa},
\end{aligned} \tag{15}
$$

where we used $g'(1) = -\kappa$ and κ is associated with the Hawking temperature, $\kappa = 4\pi T$. Note that, since the derivatives in (15) are independent of the above constant shifts, they hold even when taking different values from (13). This fact plays a crucial role in finding an asymptotic AdS geometry numerically.

In order to obtain an asymptotic AdS geometry, we should take, at the asymptotic boundary,

$$
A(0) = B(0) = 0 \quad \text{and} \quad g(0) = 1. \tag{16}
$$

In general, this condition is not consistent with the previous condition in (13) defined at the horizon. This is because there is no numerical solution interpolating these two kinds of boundary conditions. This fact implies that we have to modify one of the boundary conditions—for instance, (13). Because of the global shift symmetry explained previously, it is also possible to take arbitrary constant values instead of (13), which does not have any effect on (15). By solving equations of motion in (10) together with (15) and (16), it is possible to find consistent values at the horizon which allow for continuous interpolation. When α_i and ρ_z are given, the numerical results are as depicted in Figs. 1 and 2, where we set $L = 1$ for convenience. When the parameters are given, we plot profiles of the variables in Fig. 1. As expected, the boundary values, $A(0) = B(0) = 0$ and $g(0) = 1$, indicate that the asymptotic geometry is an AdS space.

If turning off all of the scalar fields, the gravity theory we considered reduces to a Reissner-Nordström AdS black hole which has no scalar hair or anisotropy. If turning off the dilaton field only, this theory for $\alpha_1 = \alpha_2 = \alpha$ allows the following analytic solution [44–46]:

$$
ds^2 = \frac{L^2}{z^2}(-f(z)dt^2 + f(z)^{-1}dz^2 + dx^2 + dy^2), \tag{17}
$$

with

$$
f(z) = 1 - \frac{\alpha^2}{2}z^2 - \left(1 - \frac{\alpha^2}{2} + \frac{\mu^2}{4L^2}\right)z^3 + \frac{\mu^2}{4L^2}z^4. \tag{18}
$$

In Fig. 2, we depict the horizon values relying on the parameters. The magnitudes of $A(1)$ and $\phi(1)$ decrease as

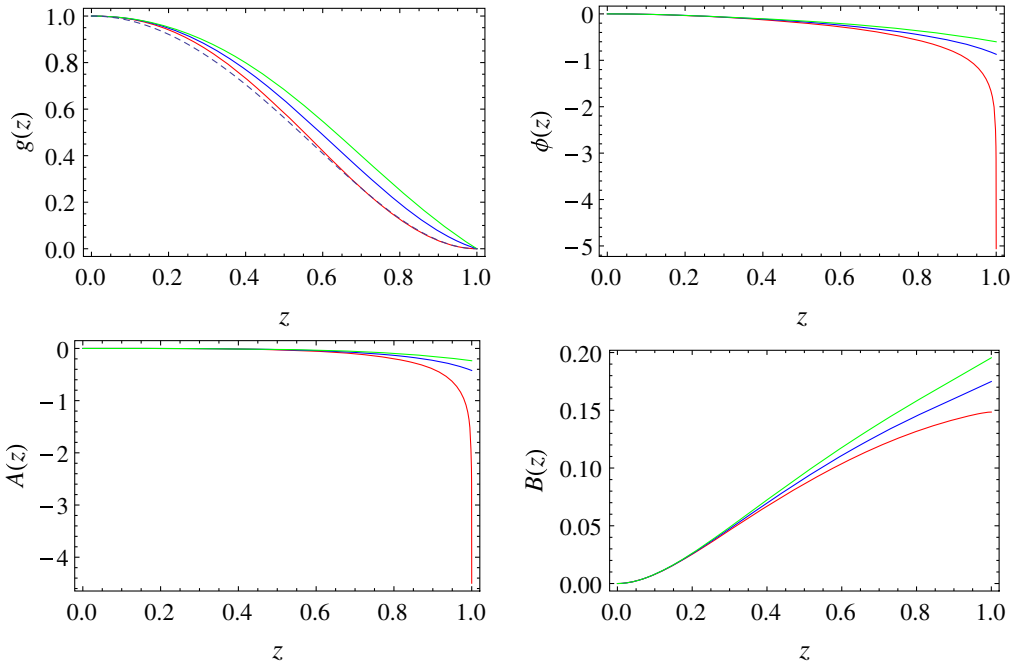

FIG. 1. Fix $\alpha_1 = 2, \alpha_2 = 2, \kappa = 2.4 \times 10^{-4}$ [lower (red) curves], 0.5 [middle (blue) curves], and 1 [upper (green) curves]. Note that the blue dashed line indicates $f(z)$ in (17).

α_2 increases, while they increase as the temperature increases. Especially for $\alpha_1 = \alpha_2 = 2$, $B(1)$ vanishes because the isotropy is restored at this point. Another interesting point we should note is that, when the temperature increases, $B(1)$ increases for $\alpha_2 < \alpha_1$, whereas it decreases for $\alpha_2 > \alpha_1$. In our work, α_i and κ are chosen as independent parameters, so ρ_z depends on these parameters. Following the AdS/CFT correspondence, the geometry we found numerically can be reinterpreted as an anisotropic medium on the dual field theory side. In this case, the anisotropy is caused by the different momentum relaxation in the x and y directions.

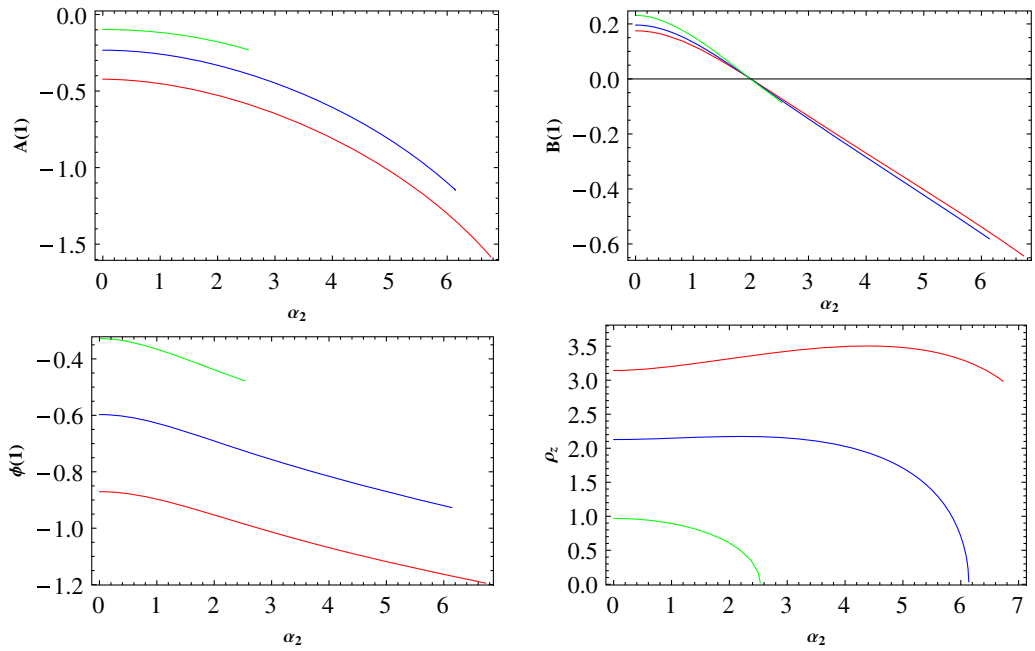

FIG. 2. The field values at the horizon for $\alpha_1 = 2$. (i) Near $\alpha_2 = 0$, $A(1)$, $B(1)$ and $\phi(1)$ are depicted for $\kappa = 0.5$ [lower (red) curves], 1 [middle (blue) curves], and 2 [upper (green) curves]. (ii) We also draw ρ_z for $\kappa = 0.5$ [upper (red) curve], 1 [middle (blue) curve], and 2 [lower (green) curve] near $\alpha_2 = 0$.

Before closing this section, let us discuss the perturbative solution near the boundary. Denoting bulk fields as Π collectively, they can be expanded into the following form near the boundary:

$$\Pi = \lim_{z\to 0}\sum_{n=0}^{\infty}\Pi^{(n)}z^n. \tag{19}$$

The perturbative solution satisfying the equations of motion in (10) are given by

$$\begin{aligned}
&A^{(0)} = B^{(0)} = \phi^{(0)} = 0, \qquad g^{(0)} = 1, \qquad B^{(1)} = \phi^{(1)} = A^{(1)} = g^{(1)} = 0,\\
&A^{(2)} = A^{(3)} = 0, \qquad \phi^{(2)} = g^{(2)} = -\frac{1}{4}(\alpha_1^2+\alpha_2^2), \qquad B^{(2)} = \frac{1}{4}(\alpha_1^2-\alpha_2^2),\\
&A^{(4)} = -\frac{1}{96}(5\alpha_1^4+6\alpha_1^2\alpha_2^2+5\alpha_2^4), \qquad \phi^{(4)} = -\frac{1}{16}(3\alpha_1^4+4\alpha_1^2\alpha_2^2+3\alpha_2^4-4\rho_z^2),\\
&g^{(4)} = \frac{1}{24}(24\rho_z^2-5\alpha_1^4-6\alpha_1^2\alpha_2^2-5\alpha_2^4),\\
&B^{(4)} = \frac{3}{16}(\alpha_1^2-\alpha_2^2),\\
&\cdots.
\end{aligned} \tag{20}$$

Above, $g^{(3)}$, $B^{(3)}$, and $\phi^{(3)}$ are undetermined integral constants which can be fixed by imposing additional boundary conditions at the horizon. This perturbative solution plays an important role in calculating the on-shell gravity action and in evaluating conductivities of the dual anisotropic medium.

III. CONDUCTIVITIES IN AN ANISOTROPIC MEDIUM

In order to investigate various conductivities of the anisotropic medium considered in the previous section, we perturb the gauge field

$$A_\mu dx^\mu \to A_t(z)dt + [\tilde{A}_x(t,z)dx + \tilde{A}_y(t,z)dy]$$

with the metric fluctuation $\tilde{g}_{ti}$ $(i,j=x,y)$,

$$g_{\mu\nu}dx^\mu dx^\nu \to \bar{g}_{\mu\nu}dx^\mu dx^\nu + \frac{2L^2}{z^2}[\tilde{g}_{tx}(t,z)dtdx + \tilde{g}_{ty}(t,z)dtdy],$$

where $\bar{g}_{\mu\nu}$ is the background metric that we found in the previous section. The other metric fluctuations, like g_{ij}, are not considered here because they are usually decoupled in the linear response theory [46–48]. Note that, since fluctuations of the axion field can be coupled to the above gauge field and metric fluctuations, one should also take into account the axion's fluctuation.

Now let us consider the following Fourier mode decompositions:

$$\tilde{A}_i(t,z) = \int_{-\infty}^{\infty}\frac{d\Omega}{2\pi}e^{-i\Omega t}A_i(z), \quad \tilde{g}_{ti}(t,z) = \int_{-\infty}^{\infty}\frac{d\Omega}{2\pi}e^{-i\Omega t}g_{ti}(z),$$

and

$$\tilde{a}_i \to \alpha_i x^i + i\int_{-\infty}^{\infty}\frac{d\Omega}{2\pi}\Omega e^{-i\Omega t}\chi_i(z), \tag{21}$$

where Ω is a dimensionless frequency defined as $\Omega = \frac{L^2}{r_h}\omega$ [20]. The fluctuations are then governed by the following equations of motion:

$$A_i'' + \left(\bar{B}_i' + \frac{g'}{g} - 2\phi'\right)A_i' + \left(\frac{\Omega^2}{g^2} - \frac{4z^2e^{2\phi-2A}\rho_z^2}{g}\right)A_i - \alpha_i \mathrm{Le}^{6\phi-A}\rho_z\chi_i' = 0, \tag{22}$$

$$\chi_i'' + \left(A' + \frac{g'}{g} - \frac{2}{z} + 4\phi'\right)\chi_i' + \frac{\Omega^2}{g^2}\chi_i - \frac{\alpha_i e^{\bar{B}_i - A}}{g^2}g_{\mathrm{ti}} = 0, \tag{23}$$

$$g_{ti}' + (\bar{B}_i' - A')g_{ti} - \frac{4e^{-A}z^2\rho_z}{L}A_i - \alpha_i g e^{4\phi}\chi_i' = 0, \tag{24}$$

where $\bar{B}_i = \{-B, B\}$ for $i = \{x, y\}$. In the above equation, the fluctuations in the x and y directions seem to be decoupled. If this is true, we can consider only the fluctuation in the x direction because the fluctuation in the y direction follows the same equation of motion, just one with a different momentum relaxation parameter. However, this is not true in this work. Since the background fields, A, B, g, and ϕ are functions of both relaxation parameters, α_x and α_y, the fluctuations in the x and y directions are implicitly coupled. Therefore, the momentum relaxation parameter in the x-direction can affect the conductivities in the y direction as well as the x direction. This implies that the anisotropic medium we considered depends nontrivially on the momentum relaxations.

In order to solve the above equations, let us first focus on the near horizon behavior of the solutions. The above equations (22)–(24) have a singularity at the horizon due to $g(1) = 0$. For a well-defined solution at the horizon, fluctuations must show appropriate singular behaviors at the horizon. Introducing new variables,

$$\hat{A}_i(z) \equiv g(z)A_i'(z), \qquad \hat{\chi}_i(z) \equiv g(z)\chi_i'(z), \tag{25}$$

and

$$A_i(z) = (1-z)^\lambda a_i(z), \qquad \hat{A}_i(z) = (1-z)^\lambda \hat{a}_i(z), \qquad g_{ti}(z) = (1-z)^\lambda \zeta_{ti}(z),$$
$$\chi_i(z) = (1-z)^\lambda \eta_i(z), \qquad \hat{\chi}_i(z) = (1-z)^\lambda \hat{\eta}_i(z),$$

with an appropriate exponent λ, the above equations in terms of new variables can be rewritten as five first-order linear differential equations in each direction:

$$\hat{a}_i' + \left(\bar{B}_i' - \frac{\lambda}{1-z} - 2\phi'\right)\hat{a}_i + \left(\frac{\Omega^2}{g} - 4z^2 e^{2\phi - 2A}\rho_z^2\right)a_i - \theta_i \rho_z L e^{6\phi - A}\hat{\eta}_i = 0, \tag{26}$$

$$a_i' - \frac{\lambda}{1-z}a_i - \frac{\hat{a}_i}{g} = 0, \tag{27}$$

$$\hat{\eta}_i' + \left(A' - \frac{\lambda}{1-z} - \frac{2}{z} + 4\phi'\right)\hat{\eta}_i + \frac{\Omega^2}{g}\eta_i - \frac{\theta_i e^{-A+\bar{B}_i}\zeta_{ti}}{g} = 0, \tag{28}$$

$$\eta_i' - \frac{\lambda}{1-z}\eta_i - \frac{\hat{\eta}_i}{g} = 0, \tag{29}$$

$$\zeta_{ti}' + \left(-A' + \bar{B}_i' - \frac{\lambda}{1-z}\right)\zeta_{ti} - \theta_i e^{4\phi}\hat{\eta}_i - \frac{4\rho_z e^{-A} z^2 a_i}{L} = 0. \tag{30}$$

At the horizon, these equations lead to the following eigenvalue equation:

$$\begin{pmatrix} 0 & -\frac{\Omega^2}{g'(1)} & 0 & 0 & 0 \\ \frac{1}{g'(1)} & 0 & 0 & 0 & 0 \\ 0 & 0 & 0 & -\frac{\Omega^2}{g'(1)} & \frac{\alpha_i e^{-A(1)-\bar{B}_i(1)}}{g'(1)} \\ 0 & 0 & \frac{1}{g'(1)} & 0 & 0 \\ 0 & 0 & 0 & 0 & 0 \end{pmatrix} \begin{pmatrix} \hat{a}_i \\ a_i \\ \hat{\eta}_i \\ \eta_i \\ \zeta_{ti} \end{pmatrix} = \lambda \begin{pmatrix} \hat{a}_i \\ a_i \\ \hat{\eta}_i \\ \eta_i \\ \zeta_{ti} \end{pmatrix}, \tag{31}$$

In each direction, this eigenvalue equation allows three degenerate eigenvalues, $\lambda = 0$ and $\lambda = \pm\frac{i\Omega}{g'(1)}$, whose eigenvectors are given by

$$\psi_0 = \begin{pmatrix} 0 \\ 0 \\ 0 \\ \frac{\theta_i e^{-A(1)+\bar{B}_i(1)}}{\Omega^2} \\ 1 \end{pmatrix}, \quad \psi_{1\pm} = \begin{pmatrix} 0 \\ 0 \\ \pm i\Omega \\ 1 \\ 0 \end{pmatrix}, \quad \psi_{2\pm} = \begin{pmatrix} \pm i\Omega \\ 1 \\ 0 \\ 0 \\ 0 \end{pmatrix}. \tag{32}$$

Here, the case with $i\lambda > 0$ satisfies an incoming boundary condition, while the solution satisfying the outgoing boundary condition appears for $i\lambda < 0$. Note that $g(z)$, on the outside of the horizon, must be positive and becomes zero at the horizon. This fact implies that $g'(1)$ is always negative, as shown in Fig. 1. Assuming that $\Omega > 0$, ψ_{1+} and ψ_{2+} correspond to eigenvectors satisfying the incoming boundary condition whose eigenvalue is given by $\lambda = \frac{i\Omega}{g'(1)}$. Removing outgoing modes at the horizon, χ_i, g_{ti}, and A_i are determined as the linear combination of incoming modes and a zero mode with three coefficients, $c_0\psi_0 + c_1\psi_{1+} + c_2\psi_{2+}$. As a consequence, solutions can be uniquely determined by fixing these three coefficients. In order to fix them, we have to impose additional boundary conditions. Imposing Dirichlet boundary conditions on χ_i, g_{ti}, and A_i at the asymptotic boundary clarifies their

boundary values and, at the same time, the fix above the coefficients.

A. Conductivities of an anisotropic medium

In the previous section, we discussed how we can obtain a numerical fluctuation solution satisfying the equations of motion and the consistent boundary conditions. In order to extract some physical information following the AdS/CFT correspondence, we need to understand further its structure near the boundary. Since $z \ll 1$ near the boundary, the numerical solution obtained in the previous section allows the following perturbative expansion:

$$\Phi = \lim_{z\to 0} \sum_{n=0}^{\infty} \Phi^{(n)} z^n, \tag{33}$$

where Φ indicates all of the fluctuations like χ_i, g_{ti}, and A_i collectively. Since three fluctuations we considered satisfy the second-order differential equations, they usually have six integral constants, $\chi_i^{(0)}$, $\chi_i^{(3)}$, $g_{ti}^{(0)}$, $g_{ti}^{(3)}$, $A_i^{(0)}$, and $A_i^{(1)}$. Following the holographic prescription, $\chi_i^{(0)}$, $g_{ti}^{(0)}$, and $A_i^{(0)}$ are mapped to sources, while $\chi_i^{(3)}$, $g_{ti}^{(3)}$, and $A_i^{(1)}$ are interpreted as vacuum expectation values of the dual operators on the dual field theory side. Specifically, $A_i^{(1)}$ and $g_{ti}^{(3)}$ are duals of the electric current, J^i, and the momentum operator, T^{ti}, respectively. Note that, because of the one constraint equation in the Einstein equation, one of them can be rewritten in terms of the others. As a consequence, only five coefficients are independent, and the remaining are usually determined by these five integral constants. More precisely, we can fix $g_{ti}^{(3)}$ in terms of the other five coefficients by solving the constraint equation

$$g_{ti}^{(3)} = \frac{4A_i^{(0)}\rho_z + 3\alpha_i L\chi_i^{(3)}}{3L}. \tag{34}$$

The other coefficients in (33) can be also fixed by five independent integral constants. Here, we present several lower order coefficients,

$$\begin{aligned}
\chi_i^{(1)} &= g_{ti}^{(1)} = 0,\\
\chi_i^{(2)} &= \frac{1}{2}(\chi_i^{(0)}\Omega^2 - \alpha_i g_{ti}^{(0)}),\\
g_{ti}^{(2)} &= \frac{1}{4}(2\alpha_i\chi_i^{(0)}\Omega^2 - \alpha_1^2 g_{ti}^{(0)} - \alpha_2^2 g_{ti}^{(0)}),\\
A_i^{(2)} &= \frac{-\Omega}{2}A_i^{(0)},\\
A_i^{(3)} &= \frac{1}{6}(-\alpha_j^2 A_i^{(1)} - \Omega^2 A_i^{(1)} - \alpha_i^2 L\rho_z g_{ti}^{(0)} + \alpha_i L\Omega^2\rho_z\chi_i^{(0)}),\\
A_i^{(4)} &= \frac{1}{24}((-1)^i(\alpha_1^2 - \alpha_2^2)A_i^{(0)}\Omega^2 + 8A_i^{(0)}\rho_z^2\\
&\quad - 6A_i^{(1)}g^{(3)} + A_i^{(0)}\Omega^4 + 6\alpha_i\rho_z L\chi_i^{(3)}),
\end{aligned} \tag{35}$$

where $i \neq j$ and $g^{(3)}$ corresponds to the third-order term of the background black hole metric factor, $g(z)$, in (7). Comparing these perturbative solutions with the previous numerical solution, it is possible to know the exact numerical values of all of the coefficients.

Knowing these coefficients exactly is important for understanding the physical properties of the dual field theory because the on-shell gravity action determined by them plays the role of a generating functional in the dual theory. Since the variation of a gravity action is not well defined, we need to add an additional boundary term called the Gibbons-Hawking term for a well-defined variation. The on-shell gravity action and the Gibbons-Hawking term are given by

$$S_{\rm on} = \int \frac{d^3x}{2\pi}\left[g_{ti}\left(-4\rho_z L e^{-A+\bar{B}_i}A_i + \frac{2e^{\bar{B}_i}L^2 g'_{\rm ti}}{z^2} - \frac{\alpha_i g L^2 e^{4\phi+\bar{B}_i}\chi_i'}{2z^2}\right) + g_{\rm ti}^2\left(-\frac{e^{\bar{B}_i}L^2A'}{z^2} + \frac{e^{\bar{B}_i}L^2\bar{B}_i'}{z^2} - \frac{e^{\bar{B}'_i}L^2 g'}{2gz^2} - \frac{e^{\bar{B}_i}L^2}{z^3}\right)\right], \tag{36}$$

$$S_{\rm GH} = -2\int \frac{d^3x}{2\pi}\sqrt{-\gamma}K, \tag{37}$$

where γ denotes an induced metric at the boundary ($z \to 0$). In general, these actions have divergent terms corresponding to UV divergences of the dual field theory. Similar to the usual quantum field theory, this should be renormalized by adding the appropriate counterterms, which is called a holographic renormalization [36,37,49–52]. Proper counterterms removing the UV divergences are given by

$$S_{\rm ct} = \int \frac{d^3x}{2\pi}\sqrt{-\gamma}\left[-\frac{4}{L} + \frac{L}{2}\sum_{i=1}^{2}\gamma^{mn}\partial_m\tilde{a}_i\partial_n\tilde{a}_i\right]. \tag{38}$$

Substituting perturbative solutions for the fluctuation's action yields the renormalized on-shell gravity action corresponding to a generating functional of the dual field theory,

$$S_{\rm re}^{(2)} = S_{\rm on} + S_{\rm GH} + S_{\rm ct} = 2\int d^2x \int \frac{d\Omega}{2\pi}\left[A_i^{(0)}A_i^{(1)} + \frac{1}{2}L^2(p_iB^{(3)} + g^{(3)})g_{ti}^{(0)}g_{ti}^{(0)} - 2L\rho_z A_i^{(0)}g_{ti}^{(0)} + \frac{3}{4}L^2\Omega^2\chi_i^{(0)}\chi_i^{(3)} - \frac{3}{4}L^2\alpha_i g_{ti}^{(0)}\chi_i^{(3)}\right], \quad (39)$$

where p_i is either 1 for $i = x$ or -1 for $i = y$. From this finite renormalized action, one can easily extract a retarded Green function following the holographic prescription [53,54].

Near the boundary, fluctuations usually allow two independent solutions,

$$\Phi_i^{\mathfrak{a}} = \mathbb{S}_i^{\mathfrak{a}} z^{3-\Delta_{\mathfrak{a}}} + \cdots + \mathbb{O}_i^{\mathfrak{a}} z^{\Delta_{\mathfrak{a}}} + \ldots, \quad (40)$$

where different fields, A_i, g_{ti}, and χ_i, are distinguished by an index $\mathfrak{a}$. Here $\Delta_{\mathfrak{a}}$ is a positive value and corresponds to the conformal dimension of the dual operator. Then the on-shell gravity action can be written in the following form:

$$S_{\rm re} = 2V\int \frac{d\Omega}{2\pi}[\bar{\mathbb{S}}_i^{\mathfrak{a}}\mathbb{A}_{\mathfrak{ab}}^{ij}(\Omega)\mathbb{S}_j^{\mathfrak{b}} + \bar{\mathbb{S}}_i^{\mathfrak{a}}\mathbb{B}_{\mathfrak{ab}}^{ij}(\Omega)\mathbb{O}_j^{\mathfrak{b}}], \quad (41)$$

where

$$\mathbb{S}_i \equiv \begin{pmatrix}\mathbb{S}_i^1\\ \mathbb{S}_i^2\\ \mathbb{S}_i^3\end{pmatrix} = \begin{pmatrix}A_i^{(0)}\\ g_{ti}^{(0)}\\ \chi_i^{(0)}\end{pmatrix}, \qquad \mathbb{O}_i \equiv \begin{pmatrix}\mathbb{O}_i^1\\ \mathbb{O}_i^2\\ \mathbb{O}_i^3\end{pmatrix} = \begin{pmatrix}A_i^{(1)}\\ g_{ti}^{(3)}\\ \chi_i^{(3)}\end{pmatrix}, \quad (42)$$

and V is the regularized spatial volume. Comparing this with the previous renormalized on-shell gravity action, we obtain

$$\mathbb{A}^{ij} = \begin{pmatrix}0 & -L\rho_z & 0\\ -L\rho_z & \frac{1}{4}L^2(g^{(3)} + p_iB^{(3)}) & 0\\ 0 & 0 & 0\end{pmatrix}\delta^{ij},$$
$$\mathbb{B}^{ij} = \begin{pmatrix}1 & 0 & 0\\ 0 & 0 & -\frac{3L^2\alpha_i}{4}\\ 0 & 0 & \frac{3L^2\Omega^2}{4}\end{pmatrix}\delta^{ij}, \quad (43)$$

and the retarded Green function is given by

$$G_{\mathfrak{ab}}^{ij} \equiv \mathbb{A}_{\mathfrak{ab}}^{ij} + \mathbb{B}_{\mathfrak{ac}}^{ik}\mathbb{O}_k^{\mathfrak{c}}(\mathbb{S}^{-1})_{\mathfrak{b}}^{j}, \quad (44)$$

where $(\mathbb{S}^{-1})_{\mathfrak{b}}^{j}$ represents $1/(\mathbb{S})_{\mathfrak{b}}^{j}$. If we focus on the gauge and metric fluctuations, the linear response to the variation of the source is given by

$$\begin{pmatrix}J^j\\ T^{tj}\end{pmatrix} = \begin{pmatrix}G_{11}^{ij} & G_{12}^{ij}\\ G_{21}^{ij} & G_{22}^{ij}\end{pmatrix}\begin{pmatrix}A_i^{(0)}\\ g_{ti}^{(0)}\end{pmatrix}, \quad (45)$$

where we have used $J^j = A^{j(1)}$ and $T^{tj} = g^{tj(3)}$.

Now let us compare this result with a known form of the linear response theory [5–7,41,42],

$$\begin{pmatrix}J^i\\ Q^i\end{pmatrix} = \begin{pmatrix}\sigma & \tilde{\alpha}T\\ \bar{\alpha}T & \bar{\kappa}T\end{pmatrix}\begin{pmatrix}E_i\\ -(\nabla_iT)/T\end{pmatrix}, \quad (46)$$

where Q^i indicates a heat current, $Q^i = T^{ti} - \mu J^i$, with a chemical potential μ defined by the boundary value of the background gauge field A_t. Note that the source terms of the fluctuations can be identified with the electric field and thermal gradient due to the diffeomorphism invariance [21,42,55]

$$E_i = i\Omega(A_i^{(0)} + \mu g_{ti}^{(0)}) \quad \text{and} \quad g_{ti}^{(0)} = -\frac{\nabla_iT}{i\Omega T}. \quad (47)$$

As a consequence, the transport coefficients can be rewritten in terms of the retarded Green functions [21]:

$$\begin{pmatrix}\sigma_{ii} & \tilde{\alpha}_{ii}T\\ \bar{\alpha}_{ii}T & \bar{\kappa}_{ii}T\end{pmatrix} = \begin{pmatrix}-\frac{iG_{11}^{ii}}{\Omega} & \frac{i(\mu G_{11}^{ii} - G_{12}^{ii})}{\Omega}\\ \frac{i(\mu G_{11}^{ii} - G_{21}^{ii})}{\Omega} & -\frac{i[G_{22}^{ii} - \tilde{G}_{22}^{ii} - \mu(G_{12}^{ii} + G_{21}^{ii} - \mu G_{11}^{ii})]}{\Omega}\end{pmatrix}. \quad (48)$$

Usually, G_{22}^{ii} does not vanish when $\Omega \to 0$. If we denote this nonzero value as $\tilde{G}_{22}^{ii}$, it yields a divergence corresponding to a contact term. Above, we subtract such a divergence for a well-defined thermal conductivity [47,56].

B. Numerical result

For simplicity, let us fix $L = 1$ and $\alpha_1 = 2$, where α_2 measures the anisotropy. After the numerical calculation following the previous procedure, we obtain electric, thermoelectric, and thermal conductivities depending on the frequencies in Figs. 3, 4, and 5, respectively. In spite of the fact that there is no explicit coupling between fluctuations in the x and y directions, these plots show a nontrivial anisotropy dependence. In other words, even when the x-direction momentum relaxation is fixed, the change of the y-direction momentum relaxation alters all of the conductivities in the x and y directions. This is because information about momentum relaxations in the x and y directions are encoded into the background geometry. For this reason, conductivities of this model are sensitive to the anisotropy (see Figs. 3, 4, and 5). Intriguingly, the electric conductivity

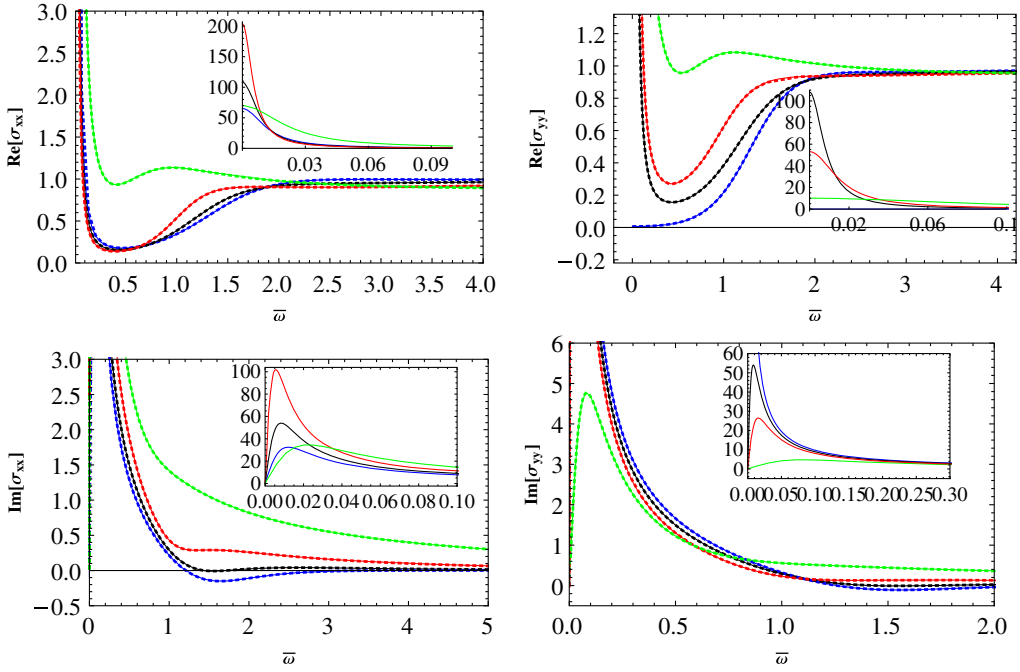

FIG. 3. The electric conductivities for $\kappa = 1$ and $\alpha_1 = 2$. Near $\bar{\omega} = 1.5$, they are depicted as the lowest (blue), lower middle (black), upper middle (red), and upper (green) curves for $\alpha_2 = 0$, 2, 4, and 6, respectively. The small figures show the finiteness of the electric conductivity at $\bar{\omega} = 0$.

in the high frequency limit seems to converge rapidly to the same value. This implies that the anisotropic effect on the electric conductivity becomes less important in the high frequency regime.

In the low frequency regime, Figs. 3, 4, and 5 show a Drude-like peak, so it would be interesting to compare it with the Drude formula

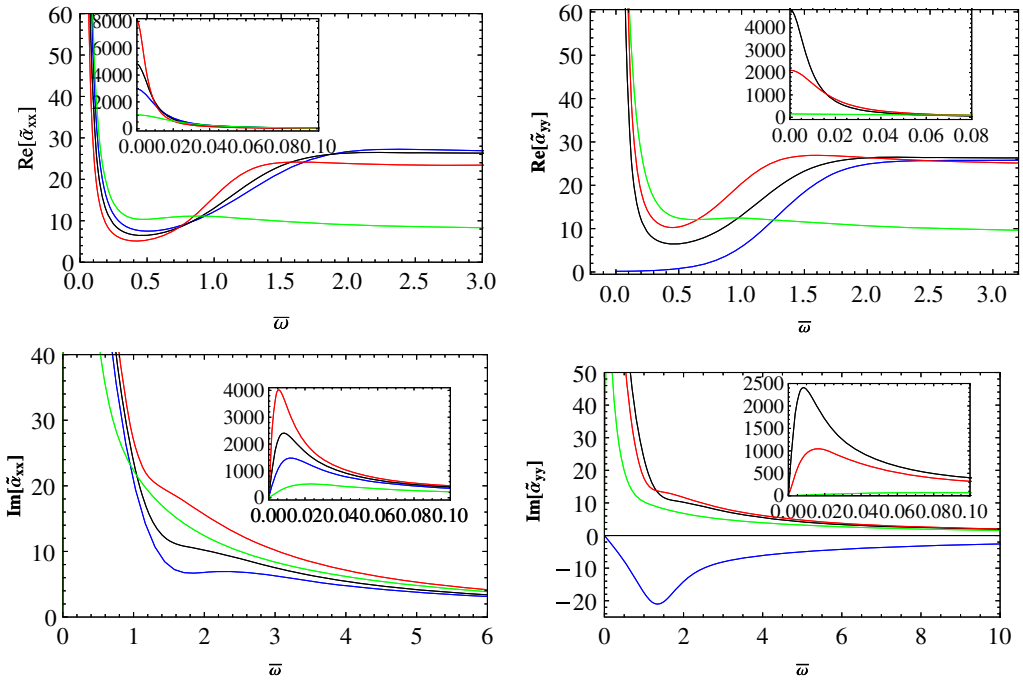

FIG. 4. The thermoelectric conductivities for $\kappa = 1$ and $\alpha_1 = 2$. $\mathrm{Re}[\bar{\alpha}_{xx}]$ at $\bar{\omega} = 1.2$ and $\mathrm{Re}[\bar{\alpha}_{yy}]$ at $\bar{\omega} = 1.5$ are represented for $\alpha_2 = 0$ [lower middle (blue) curves], 2 [upper middle (black) curves], 4 [upper (red) curves], and 6 [lowest (green) curves]. The finiteness of the imaginary parts indicates that the thermoelectric conductivities are finite in the dc limit with $\bar{\omega} = 0$.

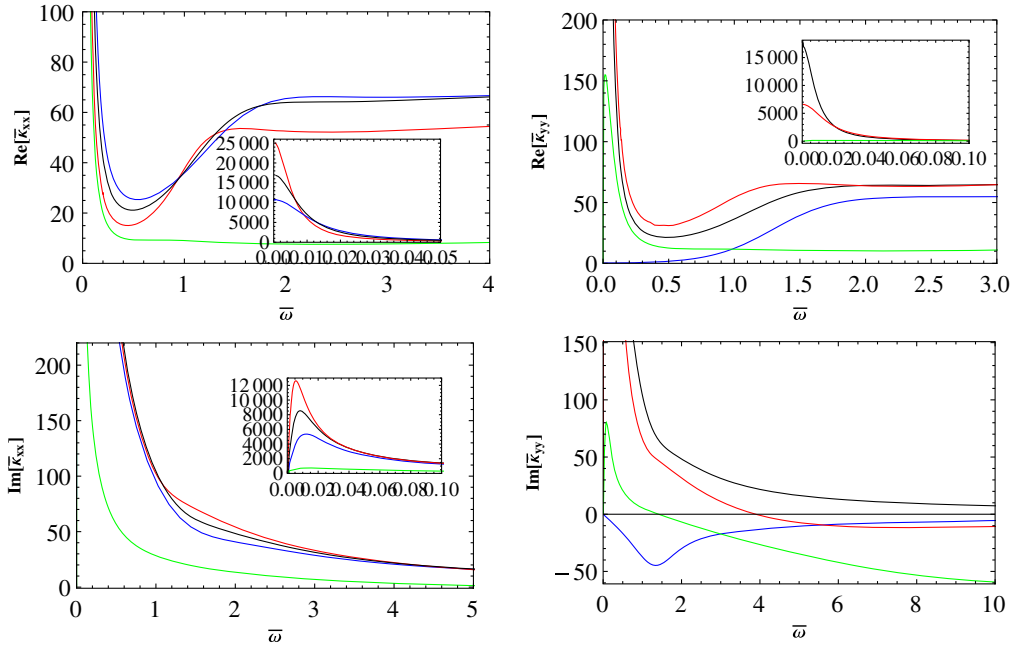

FIG. 5. The thermal conductivities for $\kappa = 1$ and $\alpha_1 = 2$. (i) Near $\bar{\omega} = 0.5$, Re$[\bar{\kappa}_{xx}]$ is represented for $\alpha_2 = 0$ [upper (blue) curve], 2 [upper middle (black) curve], 4 [lower middle (red) curve], and 6 [lowest (green) curve]. (ii) Near $\bar{\omega} = 0.5$, Re$[\bar{\kappa}_{yy}]$ is drawn for $\alpha_2 = 0$ [lowest (blue) curve], 2 [upper middle (black) curve], 4 [upper (red) curve], and 6 [lower middle (green) curve]. The finiteness of the imaginary parts indicates that the thermal conductivities are finite even at $\bar{\omega} = 0$.

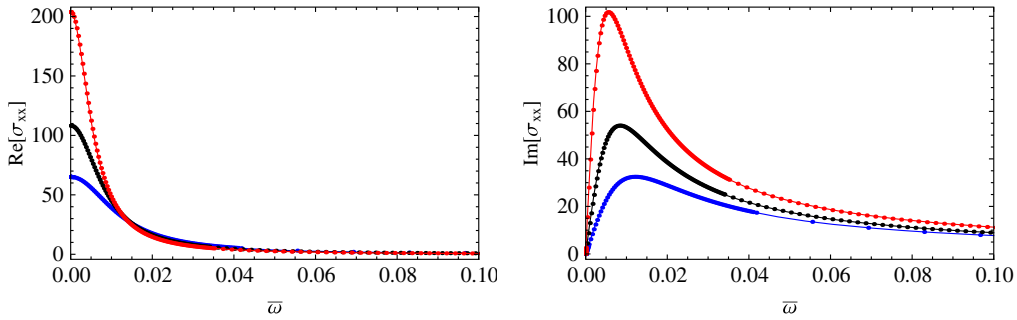

FIG. 6. Drude peak for $\alpha_1 = 2$ and $\kappa = 1$, with $\alpha_2 = 0$ [lower (blue) curves], 2 [middle (black) curves], and 4 [upper (red) curves]. Note that a solid line indicates the analytic result from the Drude formula, while dotted lines represent the numerical results.

$$\Gamma = \frac{k\tau}{1 - i\omega\tau}, \tag{49}$$

where Γ represents different kinds of conductivity. In general, the relaxation time τ and the coefficient k depend on the momentum relaxation. When α_1 is fixed, we can investigate their anisotropy dependence by varying α_2. We depict the electric conductivity, $\Gamma = \sigma_{xx}$, together

TABLE I. Parameters of the Drude formula that fit the electric conductivity well.

σ_{xx}	γ	b	c	k	τ
$\alpha_2 = 0$	2/3	2.88	−5.65	0.785	82.7
$\alpha_2 = 2$	0.89	1.3	−0.8	0.9	120
$\alpha_2 = 4$	0.626	6.87	−24.5	1.13	180

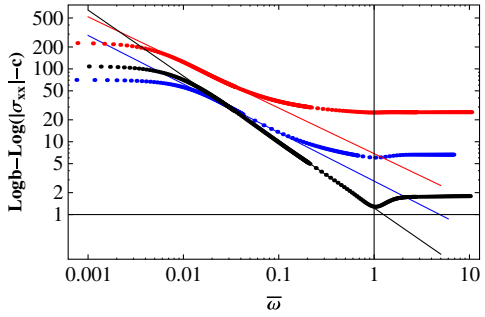

FIG. 7. The magnitude of the electric conductivity for $\alpha_1 = 2$ and $\kappa = 1$ with $\alpha_2 = 0$ [lower (blue) curve], 2 [middle (black) curve], and 4 [upper (red) curve]. The slope of the straight line denotes the power law of the electric conductivity.

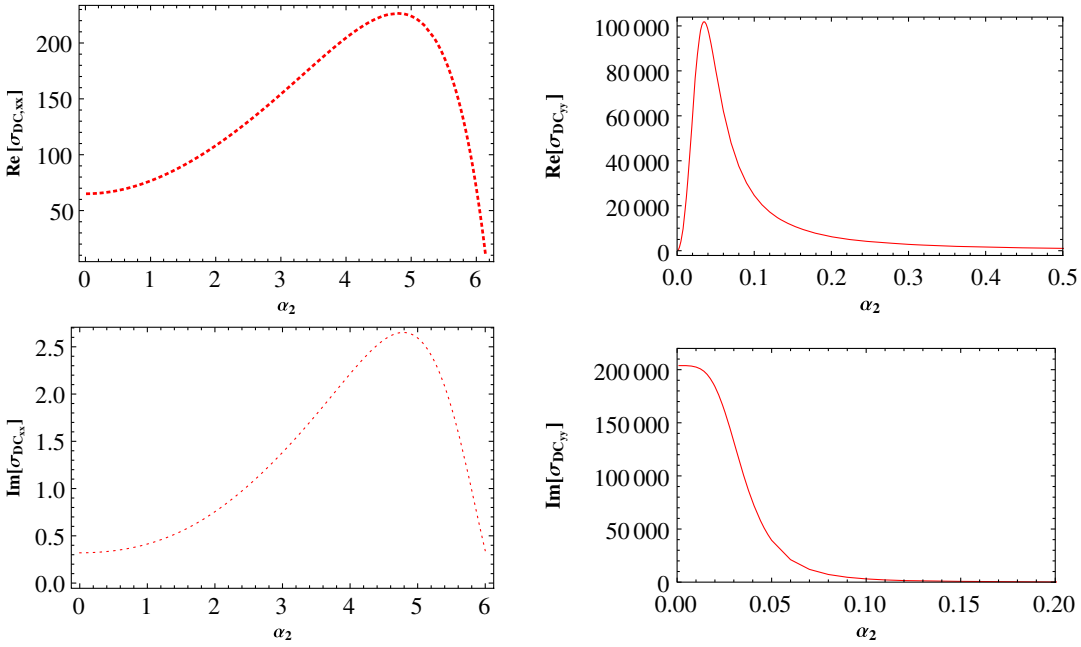

FIG. 8. dc conductivities with $\alpha_1 = 2$ and $\kappa = 1$. The range of α_2 is restricted to $0 < \alpha_2 < 6.1393$.

with the result of the Drude formula in Fig. 6. This result shows that our numerical results are perfectly matched to the Drude formula when we take the parameter values in Table I. When the momentum relaxation in the y direction increases, the relaxation time and the coefficient k in the x direction also increase. In addition, the Drude peak becomes narrow as α_2 increases within the range, $0 \leq \alpha_2 \leq 4$, similar to [20].

Now let us investigate the magnitude of the electric conductivity in an intermediate frequency regime [12]. Using the previous numerical result, the magnitude is plotted in Fig. 7, which shows a specific scaling behavior in an intermediate frequency regime. To clarify the scaling behavior, we consider the following power law behavior:

$$|\sigma| = \frac{b}{\omega^{\gamma}} + c, \tag{50}$$

where the exponent γ determines the scaling behavior. In order to fit the numerical data, we found the best parameter values in Table I. In the isotropic case, the scaling exponent is given by $\gamma = 0.89$. When the anisotropy becomes large, our result shows that the scaling exponent decreases.

Finally, let us study how the anisotropy affects the dc conductivity. As shown in Fig. 3, the low frequency behavior of the electric conductivity is sensitive to the anisotropy. We plot the dc conductivity depending on the anisotropy in Fig. 8 and its real part in Fig. 9. In Fig. 8, one can see that maximum values for x- and y-direction dc conductivities exist at certain critical frequencies. Below these critical frequencies, the x- and y-direction dc conductivities increase, whereas they decrease above the critical frequencies. In Fig. 9, one can see that the x-direction dc conductivity is the exact same as that of the y direction for $\alpha_2 = 2$. This is consistent with the previous isotropic result in that the dc conductivities in the x and y direction are finite and degenerate [14–16,43,45,46,56]. Before closing this section, it should be noticed that there seems to be an upper bound for α_2. When we solved equations for the background geometry with $\alpha_1 = 2$, we failed to find a numerical solution above $\alpha_2 \approx 6.1393$. If there is no such upper bound, the extrapolation in Fig. 9 says that the conductivity can change its sign at a certain value of α_2. However, the upper bound we found does not allow for the regime of a negative conductivity. Intriguingly, a similar behavior was recently reported in a different model with an isotropic momentum relaxation [57]. In this model, the conductivity becomes negative for a sufficiently large relaxation momentum, which leads to instability of the dual field theory. It would be interesting to investigate the instability of the present model following the method used in [57]. We leave this for future work.

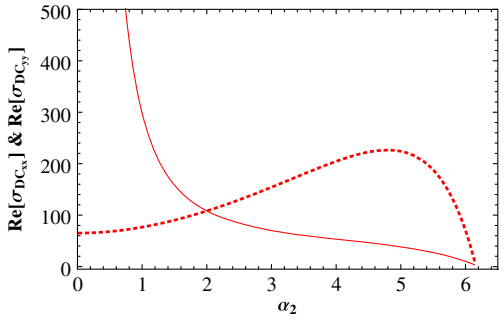

FIG. 9. α_2 dependence of dc conductivities, σ_{xx} (dotted curve) and σ_{yy} (solid curve), with $\alpha_1 = 2$ and $\kappa = 1$.

IV. CONCLUSION

In condensed matter experiments, anisotropy is one of the important ingredients. However, it is not generally easy to understand the anisotropic effect in a strongly interacting system. In this work, we tried to figure out qualitative features of the anisotropy by using the AdS/CFT correspondence. In order to mimic such an anisotropy, we considered an Einstein-Maxwell-dilaton-axion model as a dual gravity theory. In this model, the gauge and dilaton fields describe matter and a nontrivial coupling of the dual field theory. On the other hand, the momentum relaxations denoted by α_1 and α_2 were introduced to represent breaking of the translational symmetry in the x and y directions. Taking different values for α_1 and α_2 further breaks the rotational symmetry which is the origin of the anisotropy. By solving the Einstein equations, we constructed an anisotropic charged black hole solution numerically. Furthermore, we took into account the dynamics of vector fluctuations on this charged black hole, which allowed us to investigate the effect of the anisotropy on the transport coefficients, which included electric, thermoelectric, and thermal conductivities. There are several remarkable points for the linear responses in an anisotropic medium.

(i) When a momentum relaxation was turned on, we numerically showed that conductivities in the x and y directions became finite, as expected.
(ii) Although equations for vector fluctuations in the x and y directions were not coupled, we found that the y-direction momentum relaxation could affect both the x- and y-direction linear responses. On the gravity side, this is because the background geometry involves information about x- and y-direction momentum relaxations.
(iii) There exists a critical momentum relaxation at which the dc conductivity has a maximum value.
(iv) There seems to be an upper bound of the anisotropy above which the dual geometry does not exist. This upper bound does not allow a sign change of the dc conductivity.
(v) In the low frequency regime, the electric conductivity shows a Drude peak. When the x-direction momentum relaxation is fixed to be $\alpha_1 = 2$, the Drude peak becomes broader as the y-direction momentum relaxation increases.
(vi) In the intermediate frequency regime, the magnitude of the electric conductivity shows a specific scaling behavior. In comparison to the power law behavior, our results show that the critical exponent becomes smaller as the anisotropy increases.

ACKNOWLEDGMENTS

S. K. acknowledges the Korea Ministry of Science, ICT and Future Planning for the support of the Visitors Program at the Asia Pacific Center for Theoretical Physics (APCTP). We were supported by the Korea Ministry of Education, Science and Technology, Gyeongsangbuk-Do and Pohang City. B.-H. L. was supported by the National Research Foundation of Korea (NRF), funded by the Korea government (MSIP) (Grant No. 2014R1A2A1A01002306). C. P. was supported by the Basic Science Research Program through the National Research Foundation of Korea (NRF), funded by the Ministry of Education (Grant No. NRF-2013R1A1A2A10057490). We thank B. Gouteraux for pointing out the instability associated with a negative conductivity.

[1] J. M. Maldacena, The large N limit of superconformal field theories and supergravity, Int. J. Theor. Phys. **38**, 1113 (1999); Adv. Theor. Math. Phys. **2**, 231 (1998).
[2] E. Witten, Anti–de Sitter space and holography, Adv. Theor. Math. Phys. **2**, 253 (1998).
[3] E. Witten, Anti–de Sitter space, thermal phase transition, and confinement in gauge theories, Adv. Theor. Math. Phys. **2**, 505 (1998).
[4] S. S. Gubser, I. R. Klebanov, and A. M. Polyakov, Gauge theory correlators from noncritical string theory, Phys. Lett. B **428**, 105 (1998).
[5] S. A. Hartnoll, C. P. Herzog, and G. T. Horowitz, Holographic superconductors, J. High Energy Phys. 12 (2008) 015.
[6] N. Iqbal, H. Liu, and M. Mezei, Lectures on holographic non-Fermi liquids and quantum phase transitions, arXiv:1110.3814.
[7] S. A. Hartnoll, C. P. Herzog, and G. T. Horowitz, Building a Holographic Superconductor, Phys. Rev. Lett. **101**, 031601 (2008).
[8] L. Huijse, S. Sachdev, and B. Swingle, Hidden Fermi surfaces in compressible states of gauge-gravity duality, Phys. Rev. B **85**, 035121 (2012).
[9] G. T. Horowitz, J. E. Santos, and D. Tong, Optical conductivity with holographic lattices, J. High Energy Phys. 07 (2012) 168.
[10] G. T. Horowitz, J. E. Santos, and D. Tong, Further evidence for lattice-induced scaling, J. High Energy Phys. 11 (2012) 102.
[11] G. T. Horowitz and J. E. Santos, General relativity and the cuprates, J. High Energy Phys. 06 (2013) 087.
[12] Y. Ling, C. Niu, J.-P. Wu, and Z.-Y. Xian, Holographic lattice in Einstein-Maxwell-dilaton gravity, J. High Energy Phys. 11 (2013) 006.
[13] P. Chesler, A. Lucas, and S. Sachdev, Conformal field theories in a periodic potential: Results from holography and field theory, Phys. Rev. D **89**, 026005 (2014).
[14] A. Donos and J. P. Gauntlett, Thermoelectric DC conductivities from black hole horizons, J. High Energy Phys. 11 (2014) 081.

[15] A. Donos and J. P. Gauntlett, The thermoelectric properties of inhomogeneous holographic lattices, J. High Energy Phys. 01 (2015) 035.
[16] D. Vegh, Holography without translational symmetry, arXiv:1301.0537.
[17] M. Blake and D. Tong, Universal resistivity from holographic massive gravity, Phys. Rev. D **88**, 106004 (2013).
[18] R. A. Davison, Momentum relaxation in holographic massive gravity, Phys. Rev. D **88**, 086003 (2013).
[19] M. Blake, D. Tong, and D. Vegh, Holographic Lattices Give the Graviton an Effective Mass, Phys. Rev. Lett. **112**, 071602 (2014).
[20] J. i. Koga, K. Maeda, and K. Tomoda, Holographic superconductor model in a spatially anisotropic background, Phys. Rev. D **89**, 104024 (2014).
[21] K. Y. Kim, K. K. Kim, Y. Seo, and S. J. Sin, Thermoelectric conductivities at finite magnetic field and the Nernst effect, J. High Energy Phys. 07 (2015) 027.
[22] M. Taylor, Non-relativistic holography, arXiv:0812.0530.
[23] B. H. Lee, S. Nam, D. W. Pang, and C. Park, Conductivity in the anisotropic background, Phys. Rev. D **83**, 066005 (2011).
[24] D. Mateos and D. Trancanelli, Thermodynamics and instabilities of a strongly coupled anisotropic plasma, J. High Energy Phys. 07 (2011) 054.
[25] N. Iizuka and K. Maeda, Study of anisotropic black branes in asymptotically anti–de Sitter, J. High Energy Phys. 07 (2012) 129.
[26] A. Amoretti, A. Braggio, N. Maggiore, N. Magnoli, and D. Musso, Thermo-electric transport in gauge/gravity models with momentum dissipation, J. High Energy Phys. 09 (2014) 160.
[27] L. Cheng, X.-H. Ge, and Z.-Y. Sun, Thermoelectric DC conductivities with momentum dissipation from higher derivative gravity, J. High Energy Phys. 04 (2015) 135.
[28] R. A. Davison and B. Goutraux, Momentum dissipation and effective theories of coherent and incoherent transport, J. High Energy Phys. 01 (2015) 039.
[29] V. Jahnke, A. S. Misobuchi, and D. Trancanelli, Holographic renormalization and anisotropic black branes in higher curvature gravity, J. High Energy Phys. 01 (2015) 122.
[30] L. Q. Fang, X. H. Ge, J. P. Wu, and H. Q. Leng, Anisotropic Fermi surface from holography, Phys. Rev. D **91**, 126009 (2015).
[31] X. Bai, B. H. Lee, M. Park, and K. Sunly, Dynamical condensation in a holographic superconductor model with anisotropy, J. High Energy Phys. 09 (2014) 054.
[32] K. Goldstein, N. Iizuka, S. Kachru, S. Prakash, S. P. Trivedi, and A. Westphal, Holography of dyonic dilaton black branes, J. High Energy Phys. 10 (2010) 027.
[33] S. Kulkarni, B. H. Lee, C. Park, and R. Roychowdhury, Non-conformal hydrodynamics in Einstein-dilaton theory, J. High Energy Phys. 09 (2012) 004.
[34] S. Kulkarni, B. H. Lee, J. H. Oh, C. Park, and R. Roychowdhury, Transports in non-conformal holographic fluids, J. High Energy Phys. 03 (2013) 149.
[35] C. Park, Review of the holographic Lifshitz theory, Int. J. Mod. Phys. A **29**, 1430049 (2014).
[36] C. Park, Holographic aspects of a relativistic non-conformal theory, Adv. High Energy Phys. **2013**, 389541 (2013).
[37] C. Park, Massive quasinormal mode in the holographic Lifshitz theory, Phys. Rev. D **89**, 066003 (2014).
[38] B. H. Lee, C. Park, and S. J. Sin, A dual geometry of the hadron in dense matter, J. High Energy Phys. 07 (2009) 087.
[39] C. Park, Holographic symmetry energy of the nuclear matter, Phys. Lett. B **708**, 324 (2012).
[40] B. H. Lee, S. Mamedov, S. Nam, and C. Park, Holographic meson mass splitting in the nuclear matter, J. High Energy Phys. 08 (2013) 045.
[41] C. P. Herzog, Lectures on holographic superfluidity and superconductivity, J. Phys. A **42**, 343001 (2009).
[42] S. A. Hartnoll, Lectures on holographic methods for condensed matter physics, Classical Quantum Gravity **26**, 224002 (2009).
[43] B. Goutéraux, Charge transport in holography with momentum dissipation, J. High Energy Phys. 04 (2014) 181.
[44] Y. Bardoux, M. M. Caldarelli, and C. Charmousis, Shaping black holes with free fields, J. High Energy Phys. 05 (2012) 054.
[45] T. Andrade and B. Withers, A simple holographic model of momentum relaxation, J. High Energy Phys. 05 (2014) 101.
[46] K. Y. Kim, K. K. Kim, Y. Seo, and S. J. Sin, Gauge invariance and holographic renormalization, Phys. Lett. B **749**, 108 (2015).
[47] P. Kovtun, Lectures on hydrodynamic fluctuations in relativistic theories, J. Phys. A **45**, 473001 (2012).
[48] G. Policastro, D. T. Son, and A. O. Starinets, From AdS/CFT correspondence to hydrodynamics, J. High Energy Phys. 09 (2002) 043.
[49] J. de Boer, E. P. Verlinde, and H. L. Verlinde, On the holographic renormalization group, J. High Energy Phys. 08 (2000) 003.
[50] V. Balasubramanian and P. Kraus, A stress tensor for anti–de Sitter gravity, Commun. Math. Phys. **208**, 413 (1999).
[51] S. de Haro, S. N. Solodukhin, and K. Skenderis, Holographic reconstruction of space-time and renormalization in the AdS/CFT correspondence, Commun. Math. Phys. **217**, 595 (2001).
[52] C. Park, Holographic renormalization in dense medium, Adv. High Energy Phys. **2014**, 565219 (2014).
[53] G. Policastro, D. T. Son, and A. O. Starinets, The Shear Viscosity of Strongly Coupled $N = 4$ Supersymmetric Yang-Mills Plasma, Phys. Rev. Lett. **87**, 081601 (2001).
[54] G. Policastro, D. T. Son, and A. O. Starinets, From AdS/CFT correspondence to hydrodynamics. 2. Sound waves, J. High Energy Phys. 12 (2002) 054.
[55] S. A. Hartnoll and C. P. Herzog, Impure AdS/CFT correspondence, Phys. Rev. D **77**, 106009 (2008).
[56] K. Y. Kim, K. K. Kim, Y. Seo, and S. J. Sin, Coherent/incoherent metal transition in a holographic model, J. High Energy Phys. 12 (2014) 170.
[57] B. Goutéraux, E. Kiritsis, and W.-J. Li, Effective holographic theories of momentum relaxation and violation of conductivity bound, J. High Energy Phys. 04 (2016) 122.